Hot Paper

Zitierweise: *Angew. Chem. Int. Ed.* **2021**, *60*, 7553 – 7558
Internationale Ausgabe: doi.org/10.1002/anie.202014791
Deutsche Ausgabe: doi.org/10.1002/ange.202014791

Template-Mediated Control over Polymorphism in the Vapor-Assisted Formation of Zeolitic Imidazolate Framework Powders and Films

*Min Tu, Dmitry E. Kravchenko, Benzheng Xia, Víctor Rubio-Giménez, Nathalie Wauteraerts, Rhea Verbeke, Ivo F. J. Vankelecom, Timothée Stassin, Werner Egger, Marcel Dickmann, Heinz Amenitsch, and Rob Ameloot**

Abstract: *The landscape of possible polymorphs for some metal–organic frameworks (MOFs) can pose a challenge for controlling the outcome of their syntheses. Demonstrated here is the use of a template to control in the vapor-assisted formation of zeolitic imidazolate framework (ZIF) powders and thin films. Introducing a small amount of either ethanol or dimethylformamide vapor during the reaction between ZnO and 4,5-dichloroimidazole vapor results in the formation of the porous ZIF-71 phase, whereas other conditions lead to the formation of the dense ZIF-72 phase or amorphous materials. Time-resolved in situ small-angle X-ray scattering reveals that the porous phase is metastable and can be transformed into its dense polymorph. This transformation is avoided through the introduction of template vapor. The porosity of the resulting ZIF powders and films was studied by N_2 and Kr physisorption, as well as positron annihilation lifetime spectroscopy. The templating principle was demonstrated for other members of the ZIF family as well, including the ZIF-7 series, ZIF-8_Cl, and ZIF-8_Br.*

Crystalline metal–organic frameworks (MOFs) are porous materials consisting of metal ion nodes and multitopic organic linkers.[1–3] Because of their unique properties, MOFs have attracted interest for large-volume applications (e.g., catalysis, gas storage, and gas/liquid separation)[4–6] as well as miniaturized devices (e.g., low-k dielectrics, sensors).[7,8] To realize the integration of MOFs in the latter, the development of robust methods for the deposition of homogeneous thin films is a fundamental step.[7,8] We previously reported chemical vapor deposition (CVD) of MOFs, which enables the deposition of smooth and defect-free thin films on a full-wafer scale.[9,10] This MOF-CVD method relies on the conversion of a precursor layer (e.g., ZnO, CoO, CuO) by vapors of the organic linker. As an example, the prototypical zeolitic imidazolate framework 8 (ZIF-8,[11,12] $Zn(mIm)_2$, HmIm = 2-methylimidazole) can be deposited through the vapor-solid reaction of a ZnO film with HmIm vapor. This technique has been successfully implemented in the fabrication of sensors, low-k dielectrics, and gas separation membranes.[13–15]

The MOF-CVD method has been extended to a number of other MOFs (e.g., ZIF-67, MAF-6, CuBDC).[13,16–18] However, in some other cases, the original protocol results in non-porous phases. For instance, the direct vapor-solid reaction between ZnO and 4,5-dichloroimidazole (HdcIm) vapor leads to the formation of the dense ZIF-72 phase (LCS topology; *la3d*), instead of the porous ZIF-71 phase (RHO topology; *Pm3m*).[9,19,20] The topological diversity of some MOFs can pose a challenge for controlling the synthesis outcome within a landscape of possible polymorphs.[19,21,22] In solvothermal and mechanochemical MOF synthesis, template-mediated strategies have been used to control which phase forms.[22–26] In these approaches, the template arranges the framework building blocks (e.g., by ionic bonds or hydrogen bond) and thus facilitates the formation of the desired phase, even though no direct relationship might exist between the symmetry, shape, or size of the template and the pores.[23,24] In the context of MOF-CVD, this approach remains almost entirely unexplored. Nevertheless, some linkers can act as templating agents themselves during the precursor-to-MOF conversion and are removed during subsequent activation.[10,16,27,28]

Herein, we report how the addition of a template vapor during MOF-CVD enables to steer the outcome towards either porous or non-porous members of the ZIF family. Introducing ethanol (EtOH) or dimethylformamide (DMF) vapors during the reaction between ZnO and HdcIm vapor results in the formation of ZIF-71 (Scheme 1). In contrast, H_2O vapor or the absence of additives leads to the formation of ZIF-72 or amorphous products, depending on the temperature. A similar templating principle applies to the vapor-assisted formation of other members of the ZIF family.

We first used ex situ powder X-ray diffraction (PXRD) to investigate the ZnO-to-ZIF conversion by HdcIm vapor (Figure S3). In the absence of template vapors, ZIF-72 was formed at temperatures above 150 °C. Lower temperatures

[*] Dr. M. Tu, D. E. Kravchenko, B. Xia, Dr. V. Rubio-Giménez, N. Wauteraerts, Dr. R. Verbeke, Prof. I. F. J. Vankelecom, Dr. T. Stassin, Prof. R. Ameloot
Centre for Membrane Separations, Adsorption, Catalysis, and Spectroscopy (cMACS), KU Leuven—University of Leuven
Celestijnenlaan 200F, 3001 Leuven (Belgium)
E-mail: rob.ameloot@kuleuven.be

Dr. W. Egger, Dr. M. Dickmann
Department Institut für Angewandte Physik und Messtechnik LRT2, Universität der Bundeswehr München
Werner-Heisenberg-Weg 39, 85577 Neubiberg (Germany)

Dr. M. Dickmann
Heinz Maier-Leibnitz Zentrum (MLZ), Technische Universität München, Lichtenbergstraße 1, 85748 Garching (Germany)

Prof. H. Amenitsch
Institute of Inorganic Chemistry, Graz University of Technology
Stremayrgasse 9/IV, 8010 Graz (Austria)

Supporting information and the ORCID identification number(s) for the author(s) of this article can be found under: https://doi.org/10.1002/anie.202014791.

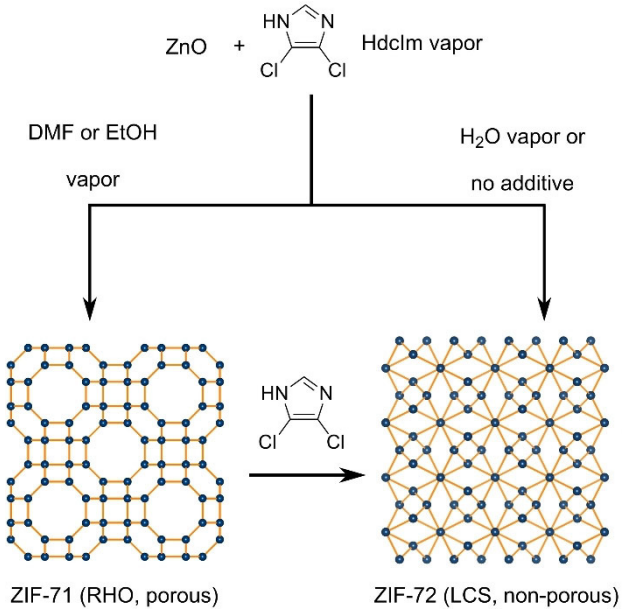

Scheme 1. Template-mediated topology control during the vapor-phase formation of MOFs. ZIF-71 is formed in the reaction between ZnO and HdcIm vapor when DMF or EtOH vapor is present. ZIF-72 is obtained in the absence of additives or when H_2O vapor is added. ZIF-71 can be transformed into ZIF-72 by HdcIm vapor. The blue sphere and orange stick represent Zn and dcIm linker, respectively.

(e.g., 110 °C) resulted in the formation of an amorphous product. When H_2O vapor was introduced during the conversion, ZIF-72 was already obtained at 110 °C. Interestingly, the introduction of DMF or EtOH vapor during the reaction resulted in the formation of ZIF-71 at the same temperature. This topology control was also realized for MOF-CVD thin films of both ZIFs, verified by grazing-incidence X-ray diffraction (GIXRD) and scanning electron microscopy (SEM; Figure S8–S11). Different types of solvent-free MOF syntheses starting from inorganic precursors have been demonstrated, including catalytically accelerated aging,[27,28] thermochemical conversion,[29,30] and mechanochemical conversion.[31,32] Some of these studies revealed the acceleration of the oxide-to-MOF conversion by H_2O vapor, due to hydroxylation of the precursor (e.g., ZnO) or protonation of the organic linker.[28,30,33] However, there has been no report on controlling polymorphism through template vapors.

To better understand the mechanism governing the topology selection, time-resolved synchrotron small-angle X-ray scattering (SAXS) was used to monitor the MOF-CVD process in situ. At 160 °C and in the absence of added vapors, the rapid formation of ZIF-71 and ZIF-72 was observed at 3 and 5 min, respectively (Figure 1 a,b). Longer reaction times resulted in the growth of ZIF-72 and the disappearance of ZIF-71 (Figure 1 a,b), indicating the transformation of the latter into the former. This phase transformation was further demonstrated by the conversion of ZIF-71 into ZIF-72 when exposed to HdcIm vapor at 130 °C (Figure 1 c, S13). In the absence of HdcIm vapor, ZIF-71 is stable up to 250 °C under identical conditions.[34] In accordance with the generally

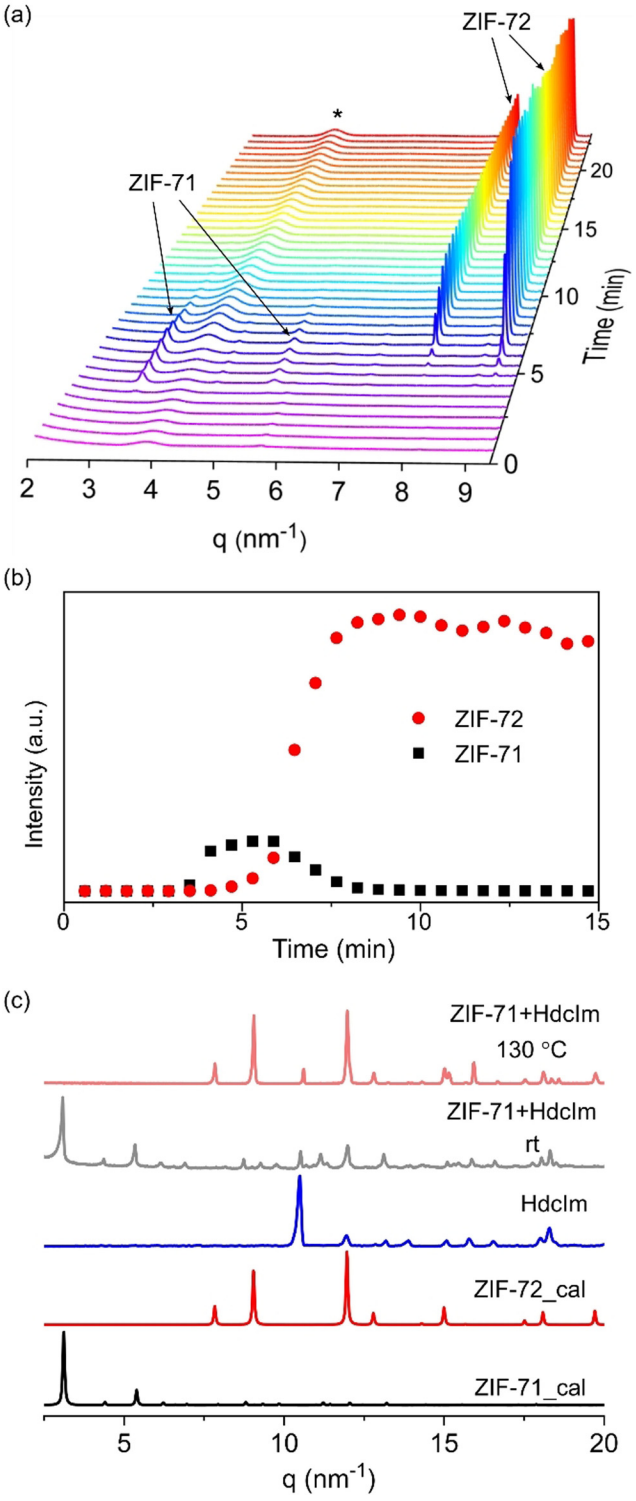

Figure 1. Phase transformation of ZIF-71 to ZIF-72 during the ZnO-to-ZIF conversion in the absence of added vapors. (a) Time-resolved in situ SAXS patterns during the reaction at 160 °C. The asterisk corresponds to parasitic scattering of the set-up, and the intensities have been normalized (b) Time-resolved changes in the integrated peak areas of the reflections at $q = 3.1$ nm^{-1} ((110) plane of ZIF-71), and $q = 9.05$ nm^{-1} ((220) plane of ZF-72). (c) PXRD patterns of the product after the reaction between ZIF-71 and HdcIm at room temperature and 130 °C for 1 day. The experimental PXRD pattern of the HdcIm linker and the calculated PXRD patterns of ZIF-71 and ZIF-72 are given for reference.

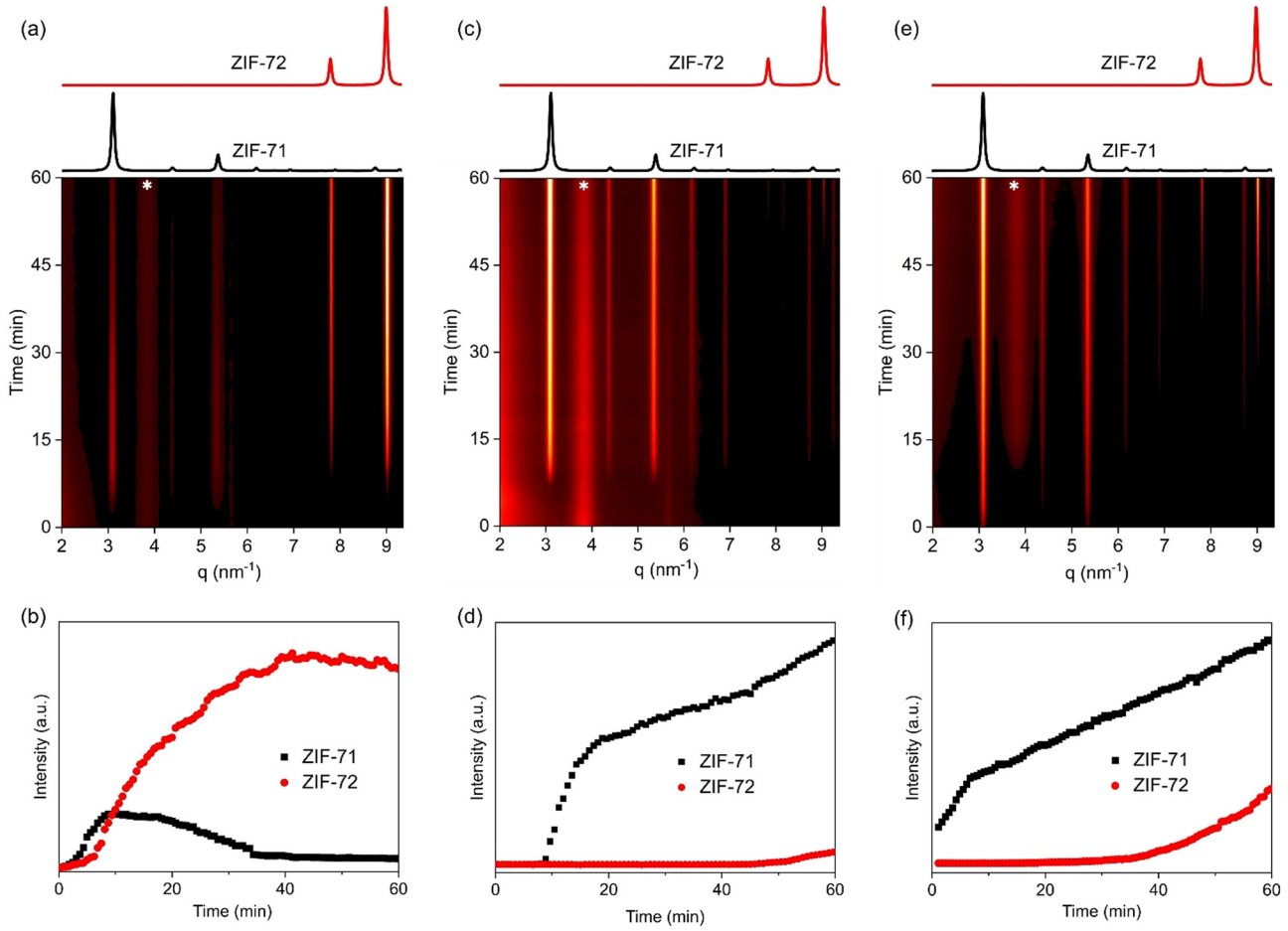

Figure 2. In situ SAXS monitoring of the template-mediated ZnO-to-ZIF conversion at 120 °C. Reaction in the presence of vapors of H_2O (a), DMF (c), and EtOH (e). The asterisk corresponds to parasitic scattering of the set-up. Time-resolved changes in the integrated peak areas of the reflections at $q = 3.1\ nm^{-1}$ ((110) plane of ZIF-71) and $q = 9.05\ nm^{-1}$ ((220) plane of ZIF-72) for the conversion using vapors of H_2O (b), DMF (d), and EtOH (f). In the presence of EtOH vapors, ZIF-71 formed already during the initial heating to 120 °C.

higher thermodynamic stability of denser phases, density functional theory (DFT) calculations revealed an energy difference of 22.3 kJ mol^{-1} between ZIF-71 and ZIF-72.[35] Following Ostwald's rule of stages,[36] the thermodynamically more stable phase (ZIF-72) formed after the metastable and kinetically preferred one (ZIF-71). Because of the same reason, exposing ZIF-71 to HdcIm vapor led to the formation of ZIF-72, through dissociative and associative linker substitution, as in vapor-phase linker exchange.[37,38] Topological transformations towards more thermodynamically stable phases have previously been observed in the mechanochemical synthesis of ZIFs.[21] However, in contrast to MOF-CVD, the mechanochemical approach moves more swiftly through the thermodynamic series, likely due to the higher energy input in the form of mechanical forces.[3]

Similar to the additive-free oxide-to-ZIF conversion at 160 °C, adding H_2O vapor at 120 °C resulted in the sequential formation of ZIF-71 and ZIF-72 (Figure 2a,b). Interestingly, when DMF or EtOH vapors were present instead, ZIF-71 formed at 120 °C, and the corresponding diffraction peaks grew continuously in intensity, while the formation of ZIF-72 was postponed significantly (> 40 min) (Figure 2c–f). These results suggest that all three vapors facilitate the oxide-to-ZIF conversion, as evidenced by the reaction proceeding at lower temperatures. However, ZIF-71 formation was preferred in the presence of DMF or EtOH vapors, while ZIF-72 was formed preferentially when H_2O vapor was present.

During solvothermal synthesis, the MOF pores are filled with solvent molecules, which can act as a template.[23] For instance, a variety of ZIF topologies have been obtained for the composition $Zn(Im)_2$ (Im = imidazolate) by using different solvents.[11,39,40] When bulky amides (e.g., dibutylformamide, dipropylformamide) instead of DMF were used, large-pore phases of $Zn(Im)_2$ can be obtained.[40] The C–H bonds of metal-coordinated imidazolate ligands were considered hydrogen bond donors.[25,41] The hydrogen bonding interaction between the solvent molecules and the metal-coordinated linkers was revealed by the single-crystal structures of several ZIFs.[11,39,40] Considering that DMF and EtOH are good hydrogen bond acceptors, they might aid in stabilizing the porous structure. In contrast, H_2O might not be able to take up this role because of the well-known hydrophobic nature of ZIF-71.[42] Previous MOF-CVD studies demonstrated that the imidazole linker itself fills the pores during

crystallization (e.g., 2-methylimidazole (HmIm) or 2-ethylimidazole (HeIm) for ZIF-8 or MAF-6, respectively).[10,16] In that case, the methyl or ethyl groups may stabilize the porous framework through $CH_3\cdots\pi$ interactions. The lack of similar interactions for HdcIm likely prevents this linker from acting as a space-filling agent on its own. In contrast, when both HdcIm and DMF (or EtOH) vapor are present during the ZnO-to-ZIF conversion, templating does occur, and formation of the porous ZIF-71 is facilitated through the resulting stabilization. This mechanism is supported by thermogravimetry-mass spectrometry (TG-MS) measurements that revealed 2 HdcIm and 10 DMF molecules per cage in ZIF-71 (Figure S17).

Although DMF or EtOH vapor acts as a template to facilitate the formation of ZIF-71, the phase transformation to ZIF-72 cannot be completely avoided at 120 °C or above (Figure 2c–f). Therefore, in situ synchrotron SAXS monitoring of the oxide-to-ZIF conversion at 90 and 105 °C was performed (Figure 3). Pure-phase ZIF-71 was obtained at 110 °C without the formation of ZIF-72, as further confirmed by ex situ PXRD for a longer reaction time (1 day; Figure S3). The conversion of ZnO to ZIF-71 in the presence of DMF and EtOH was ≈97 %, as determined by solution ^{1}H nuclear magnetic resonance spectroscopy (NMR) (Figure S21). The N_2 physisorption data of the resulting ZIF-71 exhibits a typical type I isotherm (Figure 4a), and the Brunauer-Emmett-Teller (BET) surface areas were 1030 and 1050 $m^2 g^{-1}$ when employing DMF and EtOH vapors, respectively. Notably, these values are among the highest reported, even when compared to conventional solvothermal syntheses (Table S1).

The templating approach can be transferred to the vapor-assisted synthesis of other ZIFs. The coordination of Zn^{II} and benzimidazole (HbeIm) gives rise to three phases: ZIF-7-I, -II, and -III. Two of these phases are porous (ZIF-7-I and -II) and interconvert upon adsorption/desorption of guest molecules.[43] Similar to the case of ZIF-72, the reaction between ZnO and HbeIm in a humidified environment resulted in the dense ZIF-7-III (Figure S23). In contrast, the presence of DMF vapor during the oxide-to-ZIF conversion led to the formation of the porous ZIF-7-I (Figure S23–25). ZIF-8_Cl and ZIF-8_Br are isostructural to ZIF-8, and form through the coordination of Zn^{II} to 2-chloroimidazole and 2-bromoimidazole, respectively.[44] The presence of DMF vapor during the conversion of ZnO at 110 °C induced the formation of the desired MOF phase, while no crystallization took place below 130 °C in the absence of additional vapors (Figure S26–S29). For these linkers, temperatures above 130 °C could not be tested because of thermal decomposition. The thicknesses of these ZIF films determined by ellipsometry were very close to the theoretical value expected for the full conversion of the ZnO precursor (Table S2 and Figure S31).

To investigate the porosity of the MOF films, Kr physisorption (at 77 K) and positron annihilation lifetime spectroscopy (PALS) were employed. MOF-CVD enables conformal coatings on high-aspect-ratio pillar arrays, which enables direct Kr sorption measurements on samples of practicle size (e.g., 1 cm^2 of wafer patterned as a pillar array).[9] The BET surface areas of ZIF-71, ZIF-8_Cl, and ZIF-8_Br films were 1020, 1060, and 630 $m^2 g^{-1}$, respectively

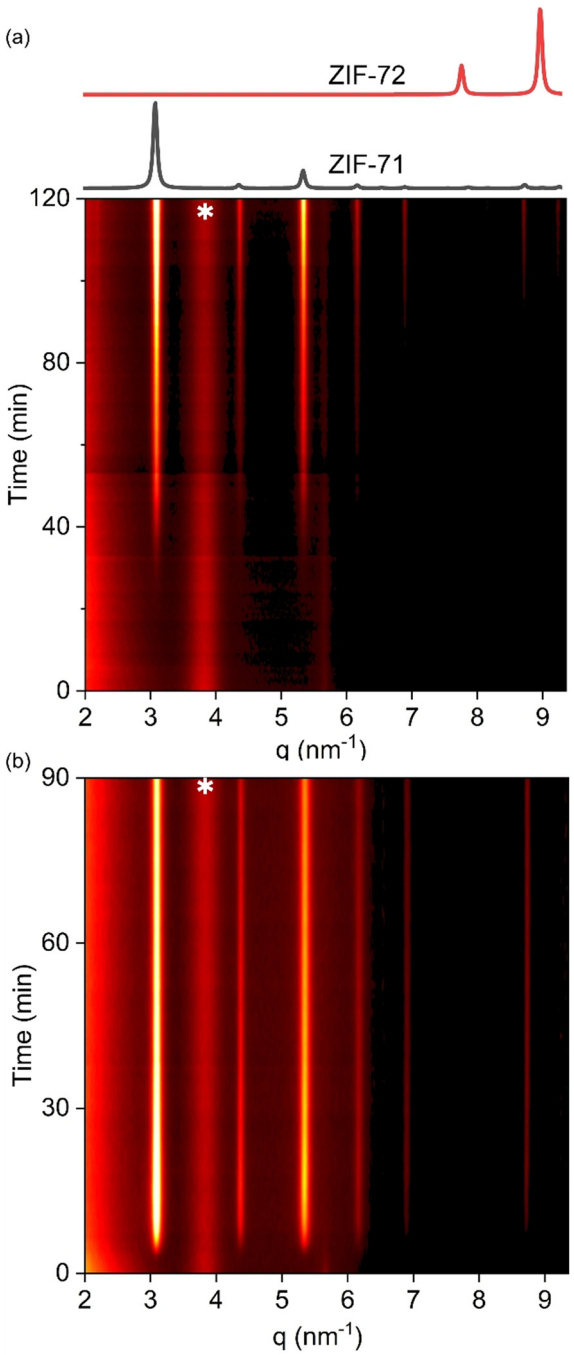

Figure 3. In situ SAXS monitoring of template-mediated MOF-CVD process below 120 °C. Time-resolved in situ synchrotron SAXS patterns during the reaction between ZnO and HdcIm vapor in the presence of DMF vapor at 105 °C (a) and EtOH vapor at 90 °C (b). The asterisk corresponds parasitic scattering of the set-up.

(Figure 4b and Table S1), which were close to the values reported for powder samples.[34,45] PALS is a technique that probes the size of free-volume elements.[46] It measures the pick-off lifetime of the *ortho*-positronium (*o*-Ps) formed upon positron implantation, which can be correlated to the pore size of the material.[46,47] ZIF-8_Cl films of different thicknesses (85, 157, and 245 nm) were studied at positron implantation energies of 1, 1.25, and 1.5 keV, corresponding

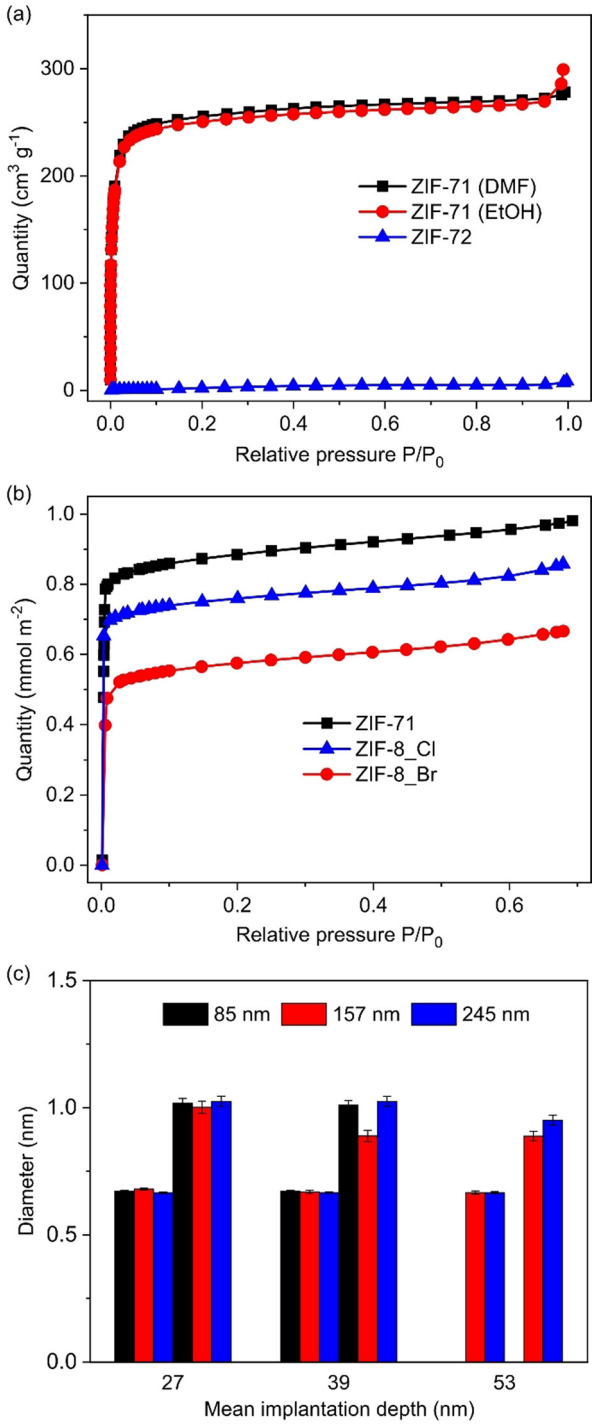

Figure 4. The porosity of MOF powders and films. a) N_2 adsorption isotherms (77 K) of ZIF-71 and ZIF-72 powder samples. b) Kr adsorption isotherms (77 K) of ZIF-71, ZIF-8_Cl, and ZIF-8_Br coatings (101, 85, and 78 nm, respectively) on high-aspect-ratio pillar arrays. c) The pore diameters of ZIF-8_Cl films with different thicknesses determined by PALS at different probe depths. The PALS measurement for the 85 nm film at mean implantation depth of 53 nm was not performed since the implantation depth exceeds the film thickness (Figure S32).

to mean implantation depths of ca. 27, 39, and 53 nm, respectively (Figure 4c, S32). Two *o*-Ps lifetimes of ca. 2.7 ns and 5.6 ns were determined for these three films at the probed depths, corresponding to pore diameters of ca. 6.8 Å and 10 Å, respectively (Figure 4c). The larger one (10 Å) was in good agreement with the crystallographic pore size, defined as the largest inscribed sphere (11.4 Å).[11] Moreover, the PALS depth-profile demonstrated the homogeneity of the porosity over the film thickness for all samples.

In conclusion, we demonstrated control over polymorphism during the template-mediated MOF-CVD process. Time-resolved in situ SAXS revealed the transition from the metastable porous phase to the thermodynamically stable dense phase during oxide-to-MOF conversion. Moreover, this phase transition could be prohibited through the introduction of a template vapor. The high porosity of the resulting MOFs in both powder and thin-film forms was demonstrated. These findings will be of considerable value in reinforcing the current understanding of the MOF-CVD synthetic approach.

Acknowledgements

R.A. acknowledges funding from the European Research Council (No. 716472, VAPORE), the Research Foundation Flanders (FWO) for funding in the research projects G083016N, G0E639N, and 1501618 N and the infrastructure project G0H0716N, and KU Leuven for funding in the research project C32/18/056. This research project has received funding from the EU's H2020 framework program for research and innovation under grant agreements 801464 FETOPEN-1–2016-2017 and 654360 NFFA-Europe (proposal IDs 462, 596, and 854). V.R.-G. acknowledges FWO for a Marie Skłodowska Curie Actions—Seal of Excellence Postdoctoral Fellowship (196025/12Z6520N). D.K. acknowledges the Marie Sklodowska Curie Training Network HYCOAT (No. 765378) for the financial support. R.V. and T.S. thank FWO for PhD fellowships (1S00917N and 1S53316N, respectively).

Conflict of interest

The authors declare no conflict of interest.

Keywords: chemical vapor deposition · metal–organic frameworks · physiosorption · template synthesis · thin films

[1] S. R. Batten, N. R. Champness, X.-M. Chen, J. Garcia-Martinez, S. Kitagawa, L. Öhrström, M. O'Keeffe, M. Paik Suh, J. Reedijk, *Pure Appl. Chem.* **2013**, *85*, 1715 – 1724.
[2] H. Furukawa, K. E. Cordova, M. O'Keeffe, O. M. Yaghi, *Science* **2013**, *341*, 1230444.
[3] T. D. Bennett, S. Horike, *Nat. Rev. Mater.* **2018**, *3*, 431 – 440.
[4] C. J. Doonan, C. J. Sumby, *CrystEngComm* **2017**, *19*, 4044 – 4048.
[5] S. Horike, S. S. Nagarkar, T. Ogawa, S. Kitagawa, *Angew. Chem. Int. Ed.* **2020**, *59*, 6652 – 6664; *Angew. Chem.* **2020**, *132*, 6716 – 6729.
[6] K. Adil, Y. Belmabkhout, R. S. Pillai, A. Cadiau, P. M. Bhatt, A. H. Assen, G. Maurin, M. Eddaoudi, *Chem. Soc. Rev.* **2017**, *46*, 3402 – 3430.

[7] I. Stassen, N. Burtch, A. Talin, P. Falcaro, M. Allendorf, R. Ameloot, *Chem. Soc. Rev.* **2017**, *46*, 3185 – 3241.
[8] M. D. Allendorf, R. Dong, X. Feng, S. Kaskel, D. Matoga, V. Stavila, *Chem. Rev.* **2020**, *120*, 8581-8640.
[9] I. Stassen, M. Styles, G. Grenci, H. V. Gorp, W. Vanderlinden, S. D. Feyter, P. Falcaro, D. D. Vos, P. Vereecken, R. Ameloot, *Nat. Mater.* **2016**, *15*, 304 – 310.
[10] A. J. Cruz, I. Stassen, M. Krishtab, K. Marcoen, T. Stassin, S. Rodríguez-Hermida, J. Teyssandier, S. Pletincx, R. Verbeke, V. Rubio-Giménez, S. Tatay, C. Martí-Gastaldo, J. Meersschaut, P. M. Vereecken, S. De Feyter, T. Hauffman, R. Ameloot, *Chem. Mater.* **2019**, *31*, 9462 – 9471.
[11] K. S. Park, Z. Ni, A. P. Côté, J. Y. Choi, R. Huang, F. J. Uribe-Romo, H. K. Chae, M. O'Keeffe, O. M. Yaghi, *Proc. Natl. Acad. Sci. USA* **2006**, *103*, 10186 – 10191.
[12] X.-C. Huang, Y.-Y. Lin, J.-P. Zhang, X.-M. Chen, *Angew. Chem. Int. Ed.* **2006**, *45*, 1557 – 1559; *Angew. Chem.* **2006**, *118*, 1587 – 1589.
[13] J.-K. Huang, N. Saito, Y. Cai, Y. Wan, C.-C. Cheng, M. Li, J. Shi, K. Tamada, V. C. Tung, S. Li, L.-J. Li, *ACS Mater. Lett.* **2020**, *2*, 485 – 491.
[14] M. Krishtab, I. Stassen, T. Stassin, A. J. Cruz, O. O. Okudur, S. Armini, C. Wilson, S. D. Gendt, R. Ameloot, *Nat. Commun.* **2019**, *10*, 3729.
[15] X. Ma, P. Kumar, N. Mittal, A. Khlyustova, P. Daoutidis, K. A. Mkhoyan, M. Tsapatsis, *Science* **2018**, *361*, 1008 – 1011.
[16] T. Stassin, I. Stassen, J. Marreiros, A. J. Cruz, R. Verbeke, M. Tu, H. Reinsch, M. Dickmann, W. Egger, I. F. J. Vankelecom, D. E. De Vos, R. Ameloot, *Chem. Mater.* **2020**, *32*, 1784 – 1793.
[17] T. Stassin, S. Rodríguez-Hermida, B. Schrode, A. J. Cruz, F. Carraro, D. Kravchenko, V. Creemers, I. Stassen, T. Hauffman, D. D. Vos, P. Falcaro, R. Resel, R. Ameloot, *Chem. Commun.* **2019**, *55*, 10056 – 10059.
[18] R. Medishetty, Z. Zhang, A. Sadlo, S. Cwik, D. Peeters, S. Henke, N. Mangayarkarasi, A. Devi, *Dalton Trans.* **2018**, *47*, 14179 – 14183.
[19] R. Banerjee, A. Phan, B. Wang, C. Knobler, H. Furukawa, M. O'Keeffe, O. M. Yaghi, *Science* **2008**, *319*, 939 – 943.
[20] M. Tu, B. Xia, D. E. Kravchenko, M. L. Tietze, A. J. Cruz, I. Stassen, T. Hauffman, J. Teyssandier, S. De Feyter, Z. Wang, R. A. Fischer, B. Marmiroli, H. Amenitsch, A. Torvisco, M. de J. Velásquez-Hernández, P. Falcaro, R. Ameloot, *Nat. Mater.* **2021**, *20*, 93 – 99.
[21] Z. Akimbekov, A. D. Katsenis, G. P. Nagabhushana, G. Ayoub, M. Arhangelskis, A. J. Morris, T. Friščić, A. Navrotsky, *J. Am. Chem. Soc.* **2017**, *139*, 7952 – 7957.
[22] M. J. Van Vleet, T. Weng, X. Li, J. R. Schmidt, *Chem. Rev.* **2018**, *118*, 3681 – 3721.
[23] D. Tanaka, S. Kitagawa, *Chem. Mater.* **2008**, *20*, 922 – 931.
[24] S. V. Kolotilov, *Theor. Exp. Chem.* **2016**, *51*, 380 – 386.
[25] I. Brekalo, C. M. Kane, A. N. Ley, J. R. Ramirez, T. Friščić, K. T. Holman, *J. Am. Chem. Soc.* **2018**, *140*, 10104 – 10108.
[26] X. Guo, S. Geng, M. Zhuo, Y. Chen, M. J. Zaworotko, P. Cheng, Z. Zhang, *Coord. Chem. Rev.* **2019**, *391*, 44 – 68.
[27] C. Mottillo, Y. Lu, M.-H. Pham, M. J. Cliffe, T.-O. Do, T. Friščić, *Green Chem.* **2013**, *15*, 2121 – 2131.
[28] M. J. Cliffe, C. Mottillo, R. S. Stein, D.-K. Bučar, T. Friščić, *Chem. Sci.* **2012**, *3*, 2495 – 2500.
[29] J.-B. Lin, R.-B. Lin, X.-N. Cheng, J.-P. Zhang, X.-M. Chen, *Chem. Commun.* **2011**, *47*, 9185 – 9187.
[30] Q. Shi, Z. Chen, Z. Song, J. Li, J. Dong, *Angew. Chem. Int. Ed.* **2011**, *50*, 672 – 675; *Angew. Chem.* **2011**, *123*, 698 – 701.
[31] T. Stolar, K. Užarević, *CrystEngComm* **2020**, *22*, 4511 – 4525.
[32] T. Friščić, C. Mottillo, H. M. Titi, *Angew. Chem. Int. Ed.* **2020**, *59*, 1018 – 1029; *Angew. Chem.* **2020**, *132*, 1030 – 1041.
[33] J. T. Newberg, C. Goodwin, C. Arble, Y. Khalifa, J. A. Boscoboinik, S. Rani, *J. Phys. Chem. B* **2018**, *122*, 472 – 478.
[34] M. E. Schweinefuß, S. Springer, I. A. Baburin, T. Hikov, K. Huber, S. Leoni, M. Wiebcke, *Dalton Trans.* **2014**, *43*, 3528 – 3536.
[35] S. Springer, I. A. Baburin, T. Heinemeyer, J. G. Schiffmann, L. van Wüllen, S. Leoni, M. Wiebcke, *CrystEngComm* **2016**, *18*, 2477 – 2489.
[36] R. A. Van Santen, *J. Phys. Chem.* **1984**, *88*, 5768 – 5769.
[37] J. Marreiros, L. V. Dommelen, G. Fleury, R. de Oliveira-Silva, T. Stassin, P. Iacomi, S. Furukawa, D. Sakellariou, P. L. Llewellyn, M. Roeffaers, R. Ameloot, *Angew. Chem. Int. Ed.* **2019**, *58*, 18471 – 18475; *Angew. Chem.* **2019**, *131*, 18642 – 18646.
[38] W. Wu, J. Su, M. Jia, Z. Li, G. Liu, W. Li, *Sci. Adv.* **2020**, *6*, eaax7270.
[39] Y.-Q. Tian, Y.-M. Zhao, Z.-X. Chen, G.-N. Zhang, L.-H. Weng, D.-Y. Zhao, *Chem. Eur. J.* **2007**, *13*, 4146 – 4154.
[40] Q. Shi, W.-J. Xu, R.-K. Huang, W.-X. Zhang, Y. Li, P. Wang, F.-N. Shi, L. Li, J. Li, J. Dong, *J. Am. Chem. Soc.* **2016**, *138*, 16232 – 16235.
[41] K. Dong, S. Zhang, J. Wang, *Chem. Commun.* **2016**, *52*, 6744 – 6764.
[42] K. Zhang, R. P. Lively, M. E. Dose, A. J. Brown, C. Zhang, J. Chung, S. Nair, W. J. Koros, R. R. Chance, *Chem. Commun.* **2013**, *49*, 3245 – 3247.
[43] P. Zhao, G. I. Lampronti, G. O. Lloyd, M. T. Wharmby, S. Facq, A. K. Cheetham, S. A. T. Redfern, *Chem. Mater.* **2014**, *26*, 1767 – 1769.
[44] K. Li, D. H. Olson, J. Seidel, T. J. Emge, H. Gong, H. Zeng, J. Li, *J. Am. Chem. Soc.* **2009**, *131*, 10368 – 10369.
[45] G. Chaplais, G. Fraux, J.-L. Paillaud, C. Marichal, H. Nouali, A. H. Fuchs, F.-X. Coudert, J. Patarin, *J. Phys. Chem. C* **2018**, *122*, 26945 – 26955.
[46] S. J. Tao, *J. Chem. Phys.* **1972**, *56*, 5499 – 5510.
[47] C. Zhou, L. Longley, A. Krajnc, G. J. Smales, A. Qiao, I. Erucar, C. M. Doherty, A. W. Thornton, A. J. Hill, C. W. Ashling, O. T. Qazvini, S. J. Lee, P. A. Chater, N. J. Terrill, A. J. Smith, Y. Yue, G. Mali, D. A. Keen, S. G. Telfer, T. D. Bennett, *Nat. Commun.* **2018**, *9*, 5042.

Manuscript received: November 4, 2020
Revised manuscript received: December 18, 2020
Accepted manuscript online: December 22, 2020
Version of record online: February 26, 2021

